6

Theoretical and Experimental Research: Diagnosis of Some Feed Kinematic Chain Structure Elements

6.1 VIBRATION AND NOISE SOURCES DURING FEED KINEMATIC CHAIN OPERATION

Modern mechanical systems have necessitated the development of research and creation of performance mechanisms. These mechanisms are capable of reducing stresses and energy loss due to friction, and producing a substantial increase of output. Integration of these mechanisms in the kinematic chains of machine tools leads to performance increase (precision, dynamical behavior, and reliability) of these chains and furthermore to the possibility of their integration in modern flexible production systems.

The helical joint with rolling elements has an outstanding place among the above-mentioned mechanisms. Introducing the rolling bodies between screw and nut, the sliding friction is replaced by rolling friction; as a result, positioning precision and output increase. Noise and vibration accompany the functioning of feed kinematic chains with the movement-transforming element-type screw-nut with balls. The noise and vibration, together with the other sources, can negatively influence

the manufacturing process, even though they are not very powerful. The noise and vibration can also negatively influence the dynamic and reliability of machine tools.

Figure 6.1 presents the main noise and vibration sources that can appear during the functioning of modern feed kinematic chains, grouped in internal and external sources depending on the origin point. In the case of external sources it can be stated with certitude that the most important weight belongs to the cutting process. In the case of internal sources, only a careful analysis can disclose the weight of each source in the global level of noise and vibrations.

A first step of this analysis is the determination by calculus of the characteristic frequencies for each mechanism that is considered as a possible source. It follows the recording of vibroacoustic signals com-

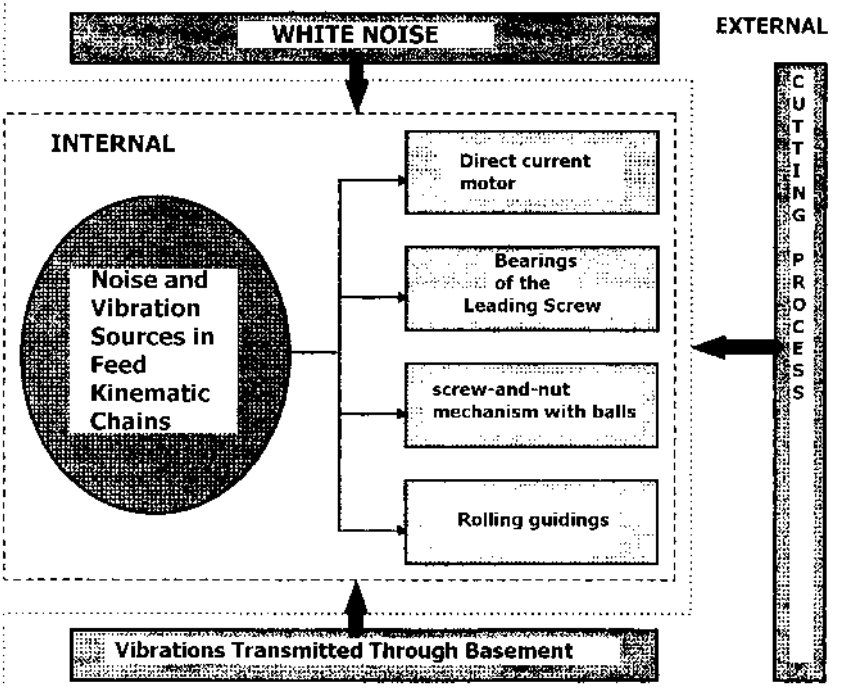

FIGURE 6.1 Main noise and vibration sources that can appear during functioning of modern feed kinematic chains.

ing from the previously mentioned sources, and the treatment of these sources using an FFT algorithm. The obtained spectrograms can indicate the weight of each characteristic frequency, and, by interpolation, the importance of each source in the assembly of the feed kinematic chain.

6.2 CALCULUS OF THE CHARACTERISTIC FREQUENCIES OF BEARINGS

A few simplifying hypotheses are necessary to calculate the characteristic frequencies from bearings:

The contact between the elements and rolling paths is done without slipping.
The influence of inertial and weight forces is negligible.
The effects of centrifugal force and gyroscopic couple are ignored.
The pressure angle α_B is considered the same for the inner and the outer rings.

If the O point from the bearing axis (Fig. 6.2) is taken as the reference point, each point of contact between the rolling body and the two rolling paths has an angular speed equal to that of the median point of the body; that is:

$$\omega_{EO} = \omega_{MO} = \omega_{IO} \tag{6.1}$$

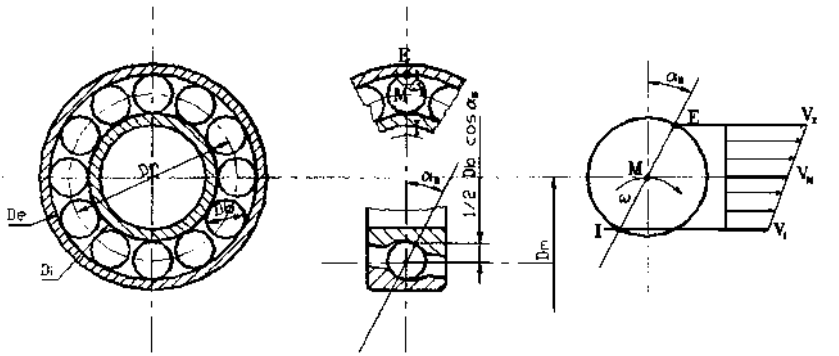

FIGURE 6.2 Bearing schematics.

The rotational speeds of the contact points can be written as

$$\begin{aligned} V_A &= \frac{1}{2}\omega_{MO}(D_m + D_b \cos\alpha_B) \\ V_I &= \frac{1}{2}\omega_{MO}(D_m - D_b \cos\alpha_B) \end{aligned} \tag{6.2}$$

If we write the angular speed of median point M function of O point as

$$\omega_{MO} = V_M / \left(\frac{1}{2} D_m\right) \tag{6.3}$$

then the above relations become:

$$\begin{aligned} V_E &= V_M \left(1 + \frac{D_b}{D_m} \cos\alpha_B\right) \\ V_I &= V_M \left(1 - \frac{D_b}{D_m} \cos\alpha_B\right) \end{aligned} \tag{6.4}$$

The E point is the center of instantaneous rotation of rolling bodies and each point of these bodies rotates around E with the angular speed ω_E. The M point results from the following formula for the rotational speed,

$$V_M = \frac{1}{2}\omega_A D_b \tag{6.5}$$

and for the I point

$$V_I = \omega_A D_b \tag{6.6}$$

This speed should be equal, according to the first hypothesis with the peripheral speed of the inner rolling path in the I point:

$$V_I = \pi n (D_m - D_b \cos\alpha_B) \tag{6.7}$$

From the last three relations, by substitution, the rotation speed of the median point M results. This speed has the expression:

$$V_M = \frac{1}{2}\pi n D_m \left(1 - \frac{D_b}{D_m} \cos\alpha_B\right) \tag{6.8}$$

The rotational peripheral speed of the bearing cage is equal to the speed of the median point M from the rolling bodies, $V_c = V_M$.

Coming back to the expressions of the rotational speeds of the points from the rolling paths, inner and outer (6.4), and replacing the

median point speed with the previously obtained relations (6.8), the new expressions result:

$$V_E = \frac{1}{2}\pi n D_m \left[1 - \left(\frac{D_b}{D_m}\cos\alpha_B\right)^2\right]$$
$$V_I = \frac{1}{2}\pi n D_m \left[\left(1 - \frac{D_b}{D_m}\cos\alpha_B\right)^2\right] \tag{6.9}$$

In this moment, the rotational frequencies characteristic to rolling bearings can be deduced:

Rotational frequency of the inner ring (rotational):

$$f_i = f_n = n/60 \tag{6.10}$$

Rotational frequency of the cage:

$$f_c = \frac{1}{2} f_n \left(1 - \frac{D_b}{D_m}\cos\alpha_B\right) \tag{6.11}$$

Rotational frequency of the rolling bodies in the cage:

$$f_m = \frac{1}{2} f_n \frac{D_m}{D_b}\left[1 - \left(\frac{D_b}{D_m}\cos\alpha_B\right)^2\right] \tag{6.12}$$

Rotational frequency of the rolling bodies on the outer ring:

$$f_E = \frac{1}{2} f_n z \left(1 - \frac{D_b}{D_m}\cos\alpha_B\right) \tag{6.13}$$

Rotational frequency of the rolling bodies on the inner ring:

$$f_I = \frac{1}{2} f_n z \left(1 + \frac{D_b}{D_m}\cos\alpha_B\right) \tag{6.14}$$

where z is the number of the rolling bodies.

In the case of using balls as rolling elements, an experimental relation exists that also permits the determination of their resonance frequency:

$$f_b = \frac{0.848}{D_b}\frac{E}{2\rho} \tag{6.15}$$

where E is the elasticity modulus and ρ is the density of ball material.

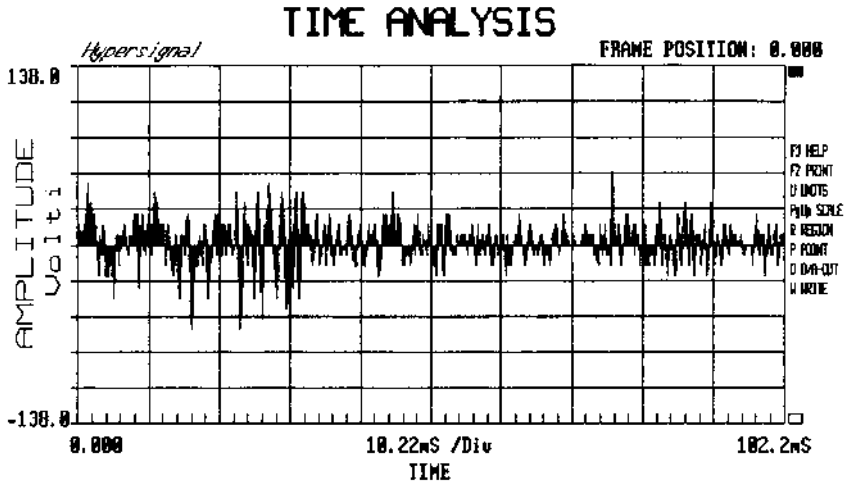

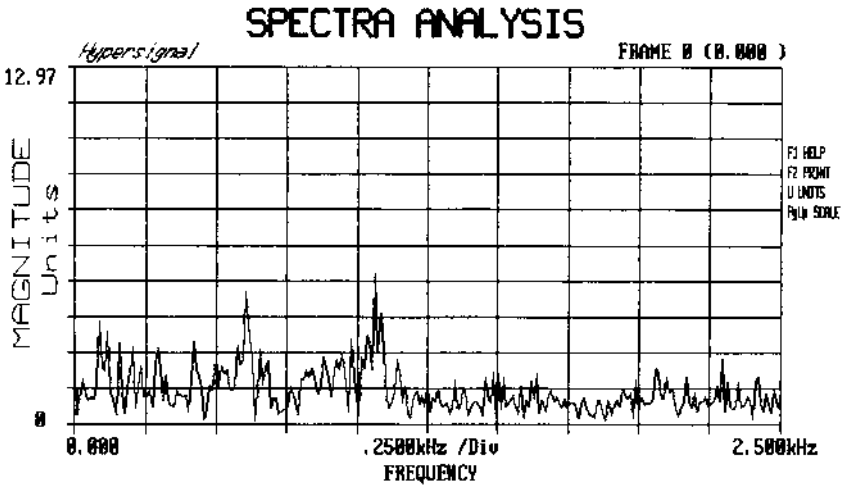

FIGURE 6.3 Vibration signal of bearing located in front of the lead screw, in perfect functioning state, recorded in time domain.

Figure 6.3a shows the vibration signal of the bearing located in front of the lead screw, in perfect functioning state, recorded in the time domain. Passing this vibration signal through a FFT of order 10, a spectrum is obtained in the frequency domain. Figure 6.3b shows this spectrum.

6.3 CALCULUS OF FREQUENCIES THAT CHARACTERIZE THE BALL SCREW-NUT MECHANISM

In the context of theoretical research regarding the vibroacoustic diagnosis of machine tools integrated in flexible manufacturing systems the following problem was posed: knowledge of characteristic frequencies of the main movement transforming mechanism in feed kinematic chains—the screw-nut with balls mechanism.

Some profoundness diagnosis methods (i.e., the evolute method) stem from the idea that a series of mechanical effects is manifesting in the frequency spectrum by large band increases near the characteristic frequencies and their harmonics from the vibrational signal. It is necessary to previously determine by theoretical procedure the characteristic frequencies, as they are not always easy to find in the standard frequency spectrum. In order to theoretically determine the characteristic frequencies an original calculus method has been set.

The study of ball movement on the rolling path is done starting from some simplifying hypothesis similar to the hypothesis presented in the previous paragraph: the contact between the balls and the rolling paths is done without sliding; and the gyroscopic couple influence, and those of inertial, weight, and centrifugal forces are ignored. To study the complex character of ball movement in the rolling channel created between screw and nut, a fixed triorthogonal axis system OXYZ (OZ direction superposes the screw axis) and a mobile system oxyz are considered. Regarding the mobile system, the oy direction is tangent to the helix described by the ball center during movement (Fig. 6.4). In the general case of ball movement on the rolling canal, it is considered that this canal is made from two trays of ogival profile, driven by axial forces of opposite directions. Two contact points will exist between the ball and the interior tray (the leading screw's canal) and one contact point between the ball and the external tray (the nut's canal). These contact points determine a plane that also passes through the center of the ball. The rolling movement of the ball will be done also around the rela-

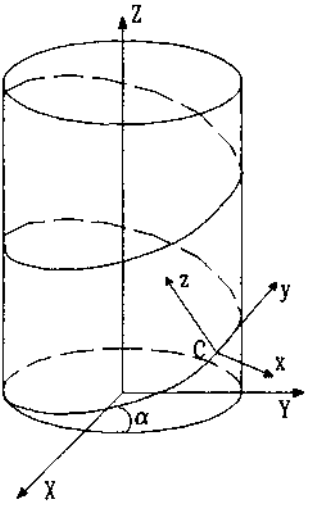

FIGURE 6.4 Helix described by the ball center during movement in the screw-and-nut mechanism.

tive instantaneous rotation axis (Δ) that passes through the previously mentioned contact points of the ball with the leading screw (Fig. 6.5),

$$P\left(\frac{D_m}{2}\cos\theta, \frac{D_m}{2}\sin\theta, \theta\frac{D_m}{2}tg\alpha\right) \tag{6.16}$$

where D_m is the medium diameter, measured to the ball center.

The tangent to the helix in the corresponding point is expressed as:

$$\vec{\tau} = \frac{d\vec{P}/d\theta}{|d\vec{P}/d\theta|} = (-\sin\theta\cos\alpha, \cos\theta\cos\alpha, \sin\alpha) \tag{6.17}$$

and the interior normal is:

$$\vec{n} = \frac{d\vec{\tau}/d\theta}{|d\vec{\tau}/d\theta|} = (-\cos\theta, -\sin\theta, \theta) \tag{6.18}$$

For the mobile axis system Oxyz, the vector of which the module is 1 for the Oy axis is $\vec{\tau}$, for the Ox axis is $-\vec{n}$, and for the Oz axis is $\vec{\nu} = -\vec{n}x\vec{\tau}$.

Let us consider now S_1 and S_2 the contact points between the ball and the leading screw, S_3 the contact point with the nut (Fig. 6.6), and

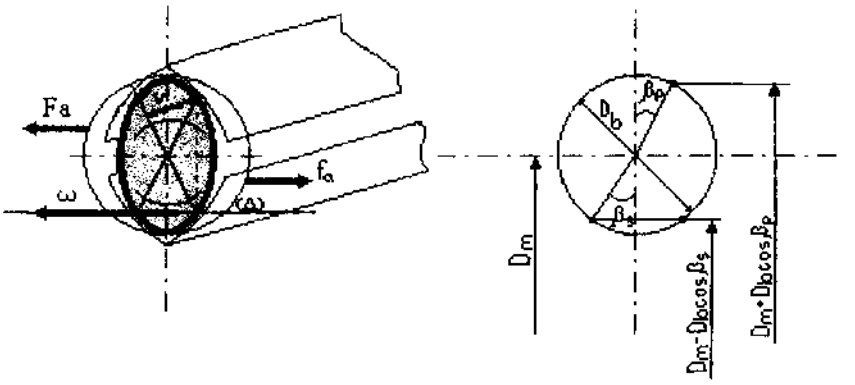

FIGURE 6.5 Rolling movement of the ball from the screw-and-nut mechanism, done also around the relative instantaneous rotation axis.

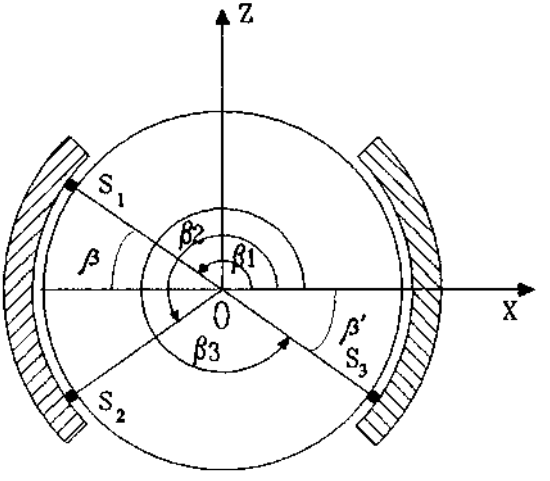

FIGURE 6.6 Contact points between the ball and leading screw, S_1 and S_2, and S_3, contact point with the nut.

D_b the ball's diameter. The location of these points depending on the mobile reference point is given by the relation:

$$\vec{r}_{Si} = -\frac{D_b}{2}\cos\beta_i\vec{n} + \frac{D_b}{2}\sin\beta_i\vec{\nu} \tag{6.19}$$

Depending on the fixed reference point, the position is $\vec{R}_{Si} = \vec{R} + \vec{r}_{Si}$, and the coordinates can be written as

$$\begin{aligned} X_{Si} &= \frac{D_m}{2}\cos\theta + \frac{D_b}{2}\cos\beta_i\cos\theta + \frac{D_b}{2}\sin\beta_i\sin\alpha\sin\theta \\ Y_{Si} &= \frac{D_m}{2}\sin\theta + D_b\cos\beta_i\sin\theta - \frac{D_b}{2}\sin\beta_i\sin\alpha\cos\theta \\ Z_{Si} &= \theta\frac{D_m}{2}tg\alpha + \frac{D_b}{2}\sin\beta_i\cos\alpha \end{aligned} \tag{6.20}$$

For S_1 and S_2 points from the screw, the speed is:

$$\begin{aligned} u_{Si} &= \dot{X}_{Si} \\ &= \dot{\theta}\left[-\frac{D_m}{2}\sin\theta - \frac{D_b}{2}\cos\beta_i\sin\theta + \frac{D_b}{2}\sin\beta_i\sin\alpha\cos\theta\right] \\ v_{Si} &= \dot{Y}_{Si} \\ &= \dot{\theta}\left[\frac{D_m}{2}\cos\theta + \frac{D_b}{2}\cos\beta_i\cos\theta + \frac{D_b}{2}\sin\beta_i\sin\alpha\sin\theta\right] \\ w_{Si} &= \dot{Z}_{Si} = \dot{\theta}\frac{D_m}{2}tg\alpha \end{aligned} \tag{6.21}$$

Simplifying the calculus for $\theta = 0$, and knowing that $\dot{\theta} = \omega_s$, the following speeds result.

$$\begin{aligned} u_{Si} &= \omega_S\frac{D_b}{2}\sin\beta_i\sin\alpha \\ v_{Si} &= \omega_S\left(\frac{D_m}{2} + \frac{D_b}{2}\cos\beta_i\right) \\ w_{Si} &= \omega_S\frac{D_m}{2}tg\alpha \qquad i = 1,2 \end{aligned} \tag{6.22}$$

The S_1 and S_2 points are usually symmetric related to the Ox axis, so it can be written:

$$\beta_1 = \pi - \beta, \qquad \beta_2 = \pi + \beta, \qquad \beta_3 = 2\pi - \beta' \tag{6.23}$$

and the previous relations become:

$$\begin{aligned}
u_S1 &= \omega\frac{D_b}{2}\sin\beta\sin\alpha \\
v_S1 &= \omega_S\left(\frac{D_m}{2}-\frac{D_b}{2}\cos\beta\right) \\
w_S1 &= \omega_S\frac{D_m}{2}tg\alpha \\
u_S2 &= -\omega_S\frac{D_b}{2}\sin\beta\sin\alpha \\
v_S2 &= \omega_S\left(\frac{D_m}{2}-\frac{D_b}{2}\cos\beta\right) \\
w_S2 &= \omega_S\frac{D_m}{2}tg\alpha
\end{aligned} \tag{6.24}$$

The S_3 point belonging to the nut has no speed (the screw is considered in a rototranslation movement). If C is the center of a ball, then its vector-radius is:

$$\vec{R}_c = \lambda_1\vec{R}_S1 + \lambda_2\vec{R}_S2 + \lambda_3\vec{R}_S3 \tag{6.25}$$

where the coefficients have the values:

$$\begin{aligned}
\lambda_1 &= \frac{\sin\dfrac{\beta+\beta'}{2}}{2\sin\beta\cos\dfrac{\beta-\beta'}{2}} \\
\lambda_2 &= \frac{\sin\dfrac{\beta-\beta'}{2}}{2\sin\beta\cos\dfrac{\beta+\beta'}{2}} \\
\lambda_3 &= \frac{\sin\beta}{\cos\beta-\cos\beta'}
\end{aligned} \tag{6.26}$$

The speed of the C center can be written as a vector

$$\vec{v}_c = \lambda_1\vec{v}_S1 + \lambda_2\vec{v}_S2 \tag{6.27}$$

or detailed on components:

$$u_C = \omega_s \frac{D_b}{2} \frac{\cos\beta' \sin\beta \sin\alpha}{\cos\beta + \cos\beta'}$$
$$v_C = \omega_s \left(\frac{D_m}{2} - \frac{D_b}{2} \cos\beta \right) \frac{\cos\beta'}{\cos\beta + \cos\beta'} \tag{6.28}$$
$$w_C = \omega_s \frac{D_m}{2} tg\alpha \frac{\cos\beta'}{\cos\beta + \cos\beta'}$$

Considering the simplifications $tg^2\alpha = 1$ and $\sin^2\alpha = 1$ ($a \ll 1$), the value of the ball center speed becomes:

$$V_C = \omega_s (D_m - D_b \cos\beta) \frac{\cos\beta'}{2(\cos\beta + \cos\beta')} \tag{6.29}$$

The relative speed of the C point in a reference point with the origin in S_1, which is united with the screw, is the difference $\Delta\vec{V} = \vec{V}_C - \vec{V}_S 1$, and the value of this speed is

$$|\Delta\vec{V}| = \omega_s (D_m - D_b \cos\beta) \frac{\cos\beta}{2(\cos\beta + \cos\beta')} \tag{6.30}$$

Knowing that the balls are consecutive, the characteristic frequencies can be determined at the moment of:

The rolling frequency of the balls on the leading screw tray:

$$f_s = \frac{\omega_s (D_m - D_b \cos\beta)}{2D_b(1 + \cos\beta')} \tag{6.31}$$

The rolling frequency of the balls on the nut's tray:

$$f_p = \frac{\omega_s (D_m - D_b \cos\beta)}{2D_b(1 + \cos\beta)} \tag{6.32}$$

The rotation frequency of the balls themselves:

$$f_b = \omega_s \frac{\cos\beta'}{\cos\beta + \cos\beta'} \tag{6.33}$$

Figure 6.7a presents the vibration signal of the screw-nut with balls mechanism, recorded in the time domain. The signal was then passed in the frequency domain through a FFT of the tenth order. Figure 6.7b presents the signal's frequency spectrum.

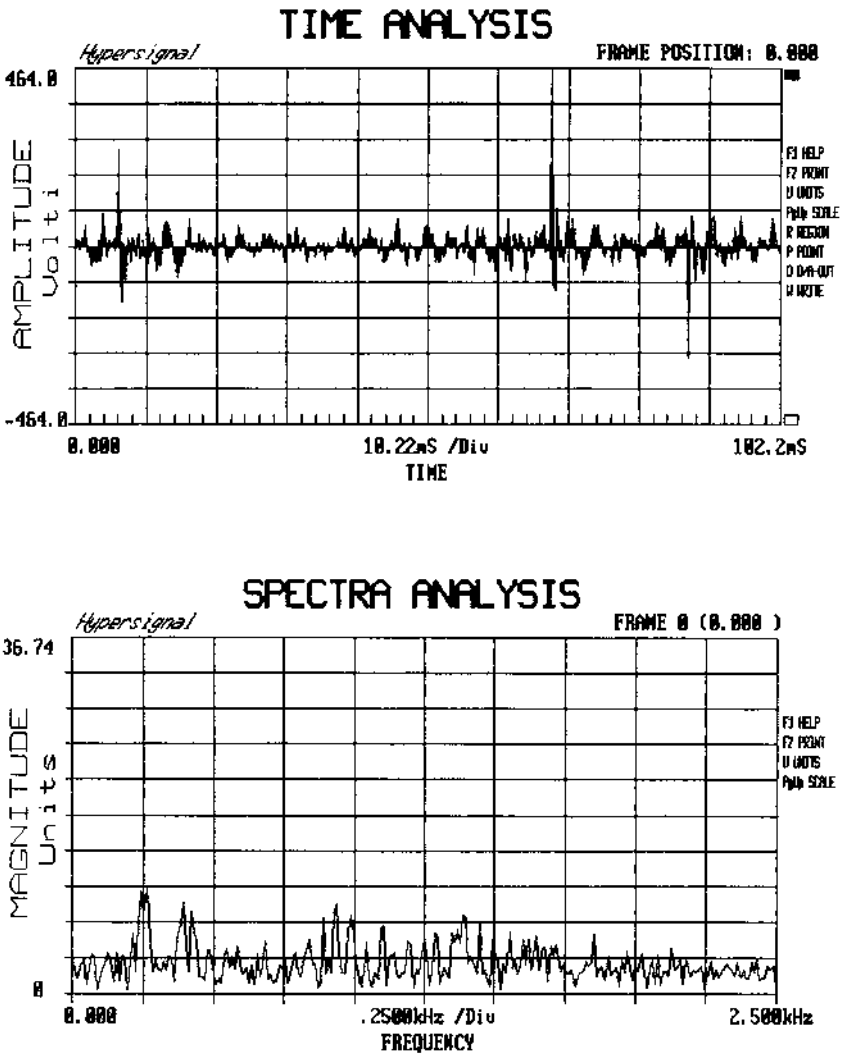

FIGURE 6.7 Vibration signal of the screw-nut with balls mechanism, recorded in time domain.

6.4 CALCULUS OF CHARACTERISTIC FREQUENCIES FOR THE TANKETTE WITH ROLLS

In the case of tankettes with rolls, the single simplifying hypothesis refers to the existence of the nonsliding contact between the rolls and the rolling paths.

Figure 6.8 shows that the tangential speeds of the rolls on the rolling paths are equal and of opposite direction, and in direct relation with the displacement speed of the mobile element (the saddle):

$$\vec{v}_s = -\vec{v}_i = \vec{V} \tag{6.34}$$

In this case, the angular speed of the balls is

$$\omega = \frac{2V}{D_r} \tag{6.35}$$

which leads to a frequency

$$f_b = \frac{V}{\pi D_r} \tag{6.36}$$

The number of the active rolls is approximated as

$$z_a = \frac{L}{D_r} \tag{6.37}$$

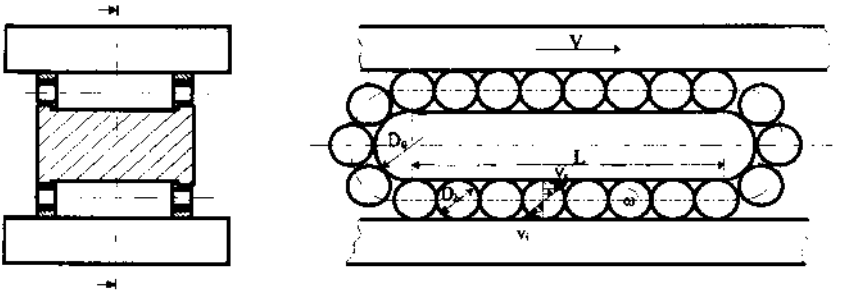

FIGURE 6.8 Tangential speeds of the rolls on the rolling paths are equal and of opposite direction.

In the above-mentioned conditions, it can be approximated as the rolling frequency of the rolls on the rolling paths (inferior and superior paths)

$$f_s = f_i = f_b z_a = \frac{VL}{\pi D_b^2} \tag{6.38}$$

or the specific rotation frequency of the rolls:

$$f_r = \frac{V}{\pi D_r} \tag{6.39}$$

Observations:

1. The identification on the basis of previous relations of a damage on the rolling element is burdened by the fact that the roll has a passive stroke bigger than that of the active stroke: $Lp = L + \pi(D_0 + D_b)$ (relative to the roll center), whose vibration signal is absent.
2. The identification of the damage from the lower rolling path (guiding) is possible only in the time interval when the guiding is covered by the tankette.

Figure 6.9a shows the vibration signal of one of the tankettes with rolls of the stand, signal recorded in the time domain. The signal was then passed in the frequency domain by a tenth-order FFT. Figure 6.9b presents the frequency spectrum of the signal.

6.5 PRELIMINARY EXPERIMENTAL RESEARCH

As shown in previous chapters, the main sources of noise and vibration in feed kinematic chains of modern construction are the bearings of the leading screw, the mechanism of movement transformation-type screw-nut with balls, and the rolling guidings of the saddle. At the same time, in the diagnostic analysis made in Chapter 4 of this book, the main sources of noise and vibration were identified as being the weak points from the feed kinematic chain structure. The diagnosis of the mechanical system of the feed kinematic chain must designate these sensible points exactly.

The common feature of these mechanisms is that they have the same principle of operation: transformation of sliding friction into rolling friction inserting intermediary elements—the rolling bodies. More than that, the damages of these mechanisms during functioning have, most

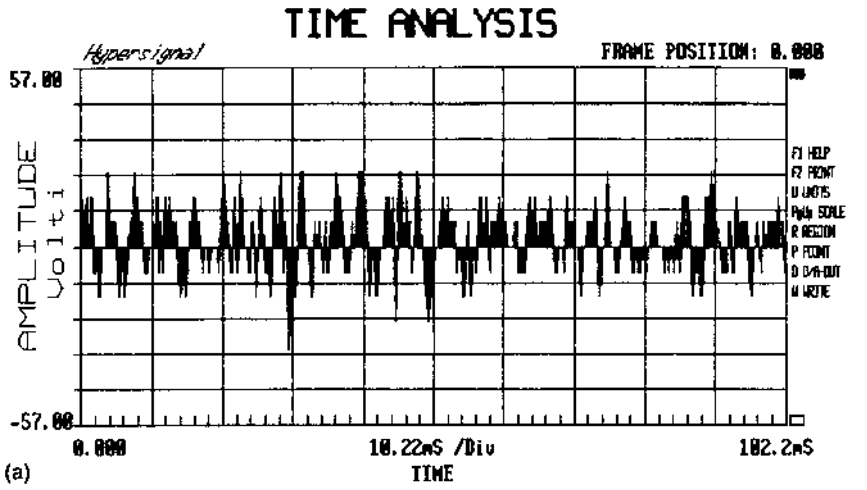

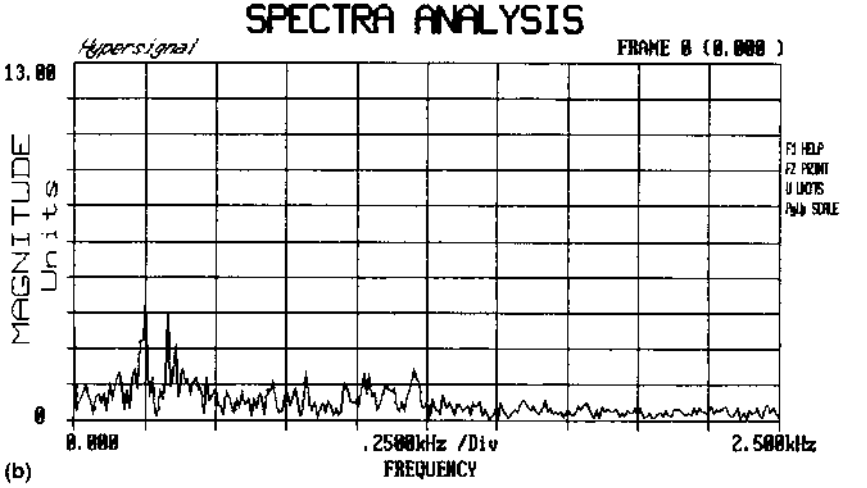

FIGURE 6.9 (a) The vibration signal of one of the tankettes with rolls of the stand, signal recorded in the time domain; (b) frequency spectrum of the signal.

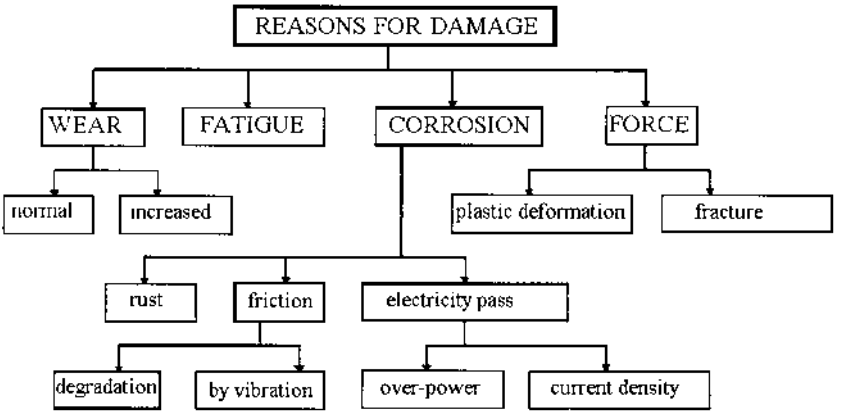

FIGURE 6.10 Causes of damage to bearings and leading screw.

often, the same causes as those generically presented in Figure 6.10. These common points allow a unitary treatment from the viewpoint of the diagnostic methods used. Thus, this chapter presents applications of the monitoring and diagnosis methods to one or another analyzed mechanism that does not exclude the use of the same methods to other mechanisms of the feed kinematic chain.

6.5.1 Experimental Research with General Use Instrumentation

The first determinations accomplished in the frame of this work were done with a general use instrumentation, of portable type, having medium performances, manufactured by RFT (Germany) and B&K (Denmark). Functioning state supervision of the 6207-P6 bearings on the test stand was done on a bearing testing machine whose kinematic schema is presented in Figure 6.11. An accelerometer B&K 4344 was connected on the cover of the tested bearing. The B&K 4344 accelerometer was connected to a general use B&K 2511 vibrometer. Peak and effective values were measured at regular intervals, each time calculating the peak factor (peak factor method). Figure 6.12 presents the results. When the bearing was dismounted, the occurrence of pitting phenomena on the rolling path of the inner ring could be noticed after the peak factor became larger than 23.

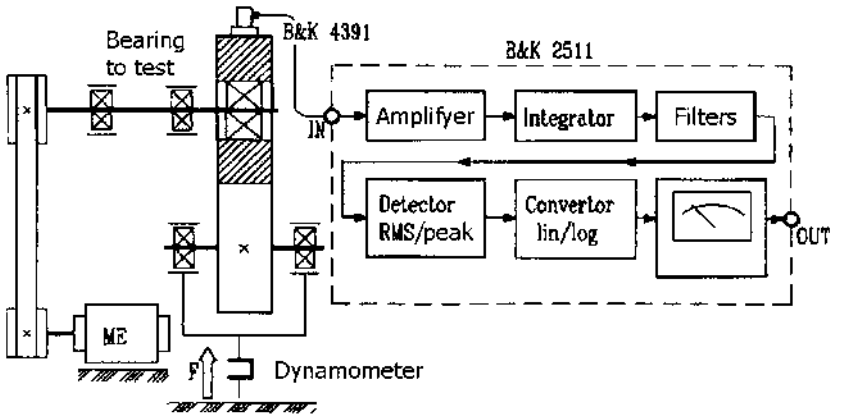

FIGURE 6.11 Kinematic schema of the bearing testing machine.

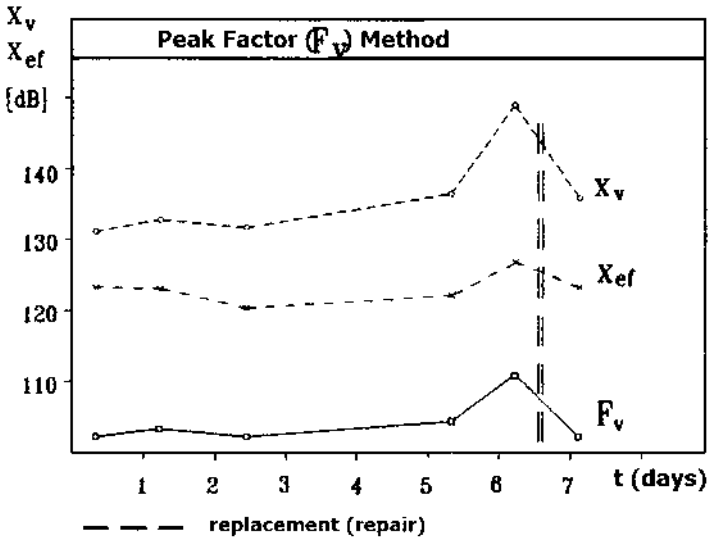

FIGURE 6.12 Peak factor method.

In parallel with measurements of vibrations, the noise emitted by bearings was also studied. For this purpose, a reverberant chamber was created setting panels around the testing machine for bearings. An RFT 0023 sonometer with a microphone with capacitor was also used. The preliminary calibration of the microphone was done with the pistophone RFT 0008. A good correlation was highlighted this way (between the limits ± 2 dB) between the level of acceleration signal of vibration and the emitted noise, as can be observed in Figure 6.13.

The technical literature claims that the peak factor method can not precisely locate the damage because it is strongly influenced by the elements of the mechanical transmission of movement. This statement was tested by remounting the fault bearing on the test stand, at the entering end of the leading screw. Vibration measurements were done using the same equipment as used for the previous experiments (peak value and effective value of acceleration signal had been done), to both bearing cases of the leading screw. The peak factor was calculated, with the result that the difference between calculated value for the case with the fault bearing and the case with the good bearing was only of one unit, which confirmed the imprecision of source localization using the peak factor method.

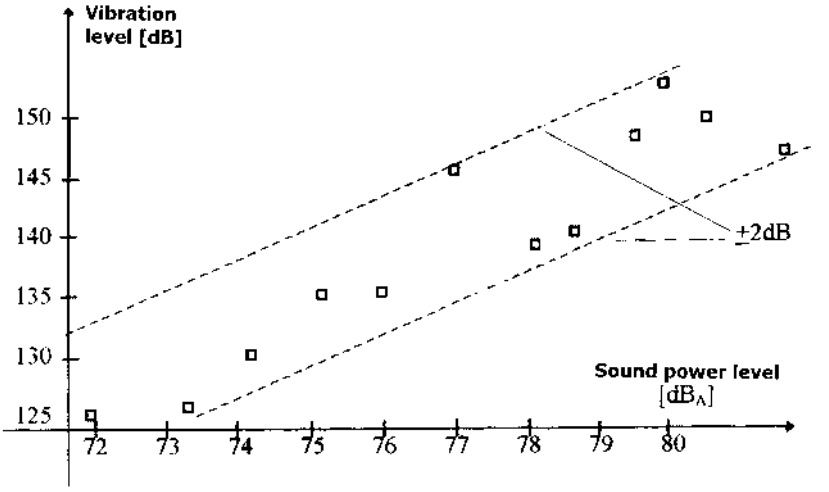

FIGURE 6.13 Good correlation between level of vibration acceleration signal and emitted noise.

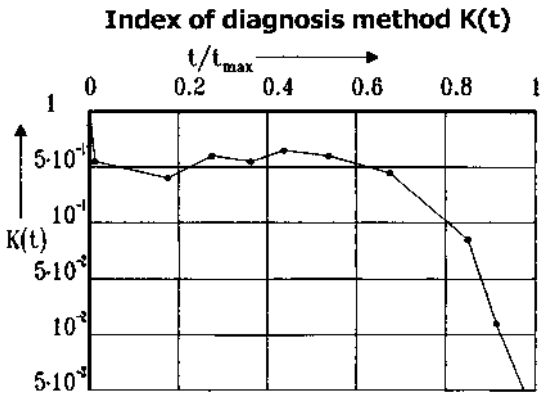

FIGURE 6.14 Method of diagnosis index has indicated the appearance of the injurious process and of the damage before the peak factor method.

After the experimental determinations, it can be noticed that the peak factor method is simple, easy to handle, and a method that utilizes general equipment. This method is useful especially in the case of monitoring a large number of measuring points, when an early warning is not required, and the consequences of the damage are not considerable. In particular situations, the peak factor method can be very well completed by a profoundness diagnosis method such as, for example, Cepstrum analysis.

The diagnosis index method was applied in parallel with the peak factor method on the 6207-P6 bearing tested on a bearings' testing machine. A first determination of statistical magnitudes that characterize the vibration signal for the bearing in perfect functioning state was useful to identify the reference and effective values of the signal. It is necessary to know these values because the diagnosis method is of "with normalization" type, which means the connection to the reference values. The diagnostic index method has indicated the appearance of the injurious process and of the damage before the peak factor method (Fig. 6.14).

6.5.2 Experimental Research Using Frequency Analysis

A new series of experiments was done after buying an assisted system of data acquisition, which is a process manufactured by the firm S.C. Emco S.A. This system captures vibration signals and process and has as

components (Fig. 6.15) a commanded load amplifier (A), for transducers of piezoelectric type, a block of simultaneous acquisition with 16 channels (B), and an interface of 8 bits for a computer (C) having a minimum configuration of 286 XT, 1 Mb RAM, and a VGA monitor. The software that governs this system (VIB-01, then VIB-02 version) was adapted to the requests of monitoring and diagnosis together with the specialists of Emco.

Hypersignal application of the firm Hyperception was adapted later to the above-mentioned system only for signal processing.

This previously mentioned software is powerful enough to allow processing the signal in the time domain, passing the signal in the frequency domain using a fast Fourier transform and multiple transformations in the frequency domain.

Several options exist in the time domain: display the captured signal (waveform display or digital oscilloscope); define and use FIR (finite impulse response) and IIR (infinite impulse response) filters; use of convolution, correlation, and autocorrelation functions; and fast Fourier transformation; and in the frequency domain: amplitude representations and phase-frequency representations, respectively; power spectrum; spectrograms in two and three dimensions, respectively; pole-zero diagram;

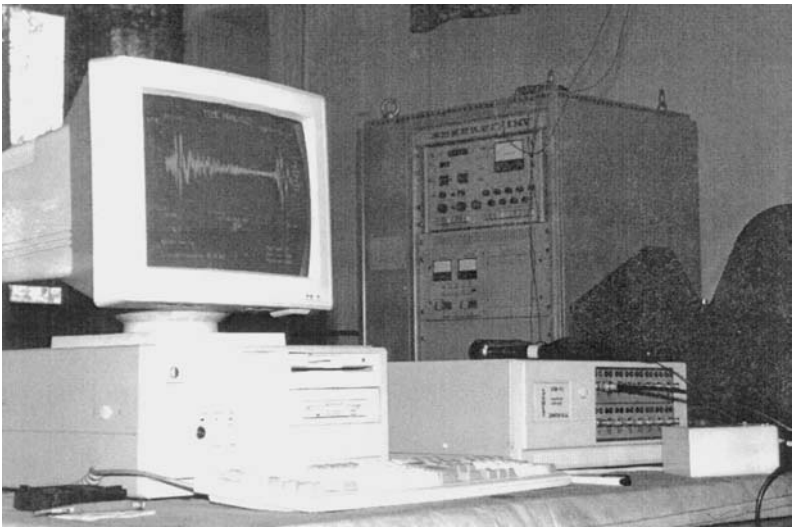

FIGURE 6.15 System of data acquisition.

transfer function for two signals; and inverse fast Fourier transformation (IFFT).

The Emco system of data acquisition and process, assisted by computer through VIB-02 application has been used for detection of a damage on the guidings with roll tankettes of the stand, by the Kurtosis method (Fig. 6.16). The simulated damage was the occurrence of pitting phenomena on the inferior rolling path of the tankettes. A B&K 4344 accelerometer was fixed on the longitudinal saddle in the nearest neighborhood of a tankette. The electronic block that processes the captured signal to calculate the Kurtosis index value was presented in Chapter 3 of this book (Fig. 3.4). A block of graphical process was attached to the electronic block to visualize the vibration signal and the probability density of the signal's amplitude.

Figures 6.17a and b present the vibration's acceleration and the probability density of the amplitude of this signal for guiding in a good functioning state. Figures 6.18a and b present the same thing as Figure 6.17 but for the damaged guiding. The modifications of the acceleration signal of vibration, and, more important, of the probability density

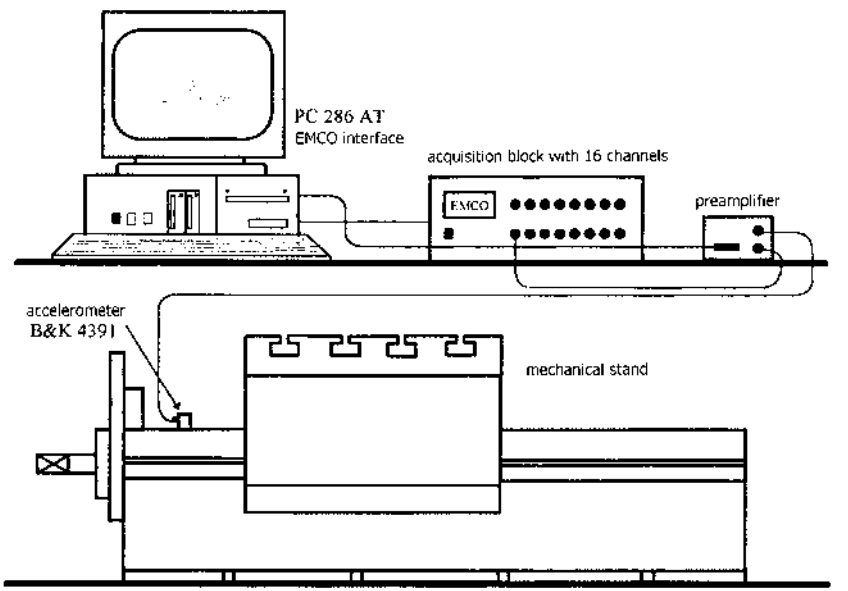

FIGURE 6.16 Emco system of data acquisition and process, assisted by computer through VIB-02 application.

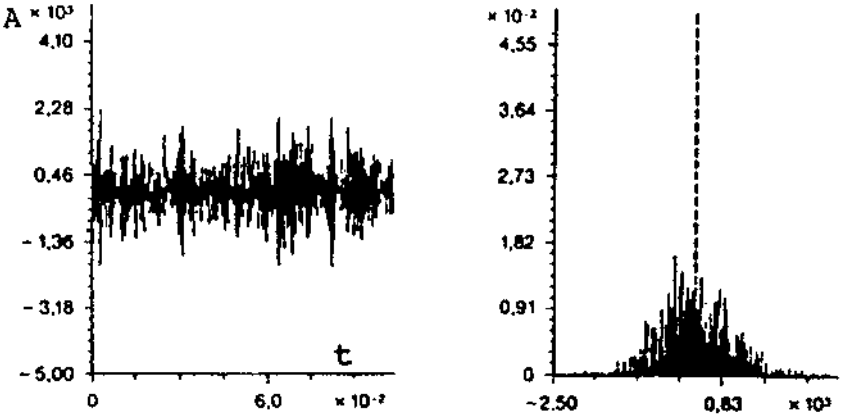

FIGURE 6.17 Vibration's acceleration and amplitude probability density of this signal for guiding in a good functioning state.

function can be monitored. In relation to this function, the calculated Kurtosis factor is, in the first case, $\beta_2 = 3.48$, and in the second case $\beta_2 = 9.34$.

Determination by calculus of characteristic frequencies of some elements from the kinematic chain structure of machine tools allows the identification of certain types of faults by analysis of the frequency spec-

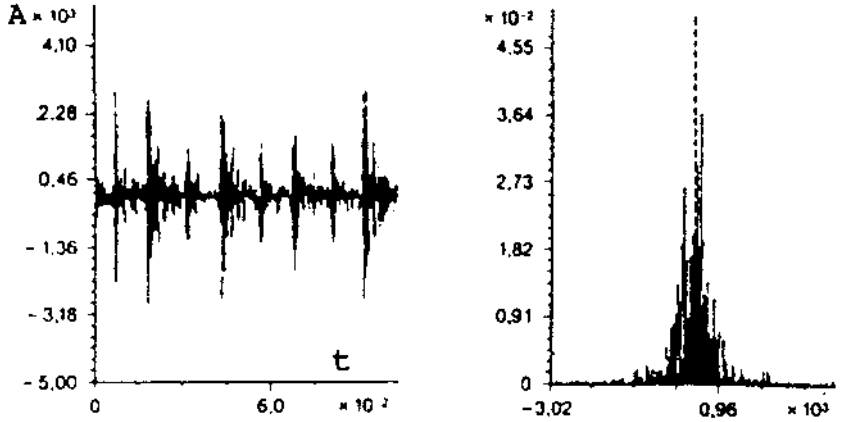

FIGURE 6.18 Vibration's acceleration and the amplitude probability density of this signal for the damaged guiding.

trum. As presented before, the most useful representation in this case is the power spectrum, which is correlated directly with the vibration signal energy.

The bearing testing machine presented in Figure 6.11 was used again to identify the faults that occur in the functioning of radial ball bearings, through power spectrum analysis. This time, the Emco system with the Hypersignal software was used to capture and process the vibrator signal from the case of the radial single-row ball bearings 6207 and 6209.

Table 6.1 presents the constructive parameters considered for the calculus of characteristic frequencies of 6207 and 6209 bearings, and also the values of these frequencies, depending on rotational frequency f_n of the inner ring. The characteristic frequencies were calculated using the relations (6.11) to (6.13) previously presented.

Figure 6.19 presents a power spectrum that was drawn on a 6207 bearing in a state of perfect functioning. This power spectrum can be considered as the reference spectrum. After rolling a few days in the absence of any lubricant, the first signs of damage occurred and the interpretation of the power spectrum of the captured vibrational signal could be started (Fig. 6.20). It can be noticed that the peak of greatest amplitude corresponds to 78.1 Hz frequency.

Considering that the rotational speed of the inner ring is equal to the rotational speed of synchronism of the driving electrical motor ($n_{ME} = 1420$ rpm), the frequency of the inner ring is $f_n = 23.66$ Hz. In these conditions, the frequency characteristic to balls rolling on the external tray is equal to $f_e = 77.42$ Hz, calculated with the relation to Table 6.1. The calculus of the other frequencies characteristic to bearing functioning did not offer any similitude with the significant increases of amplitude in the power spectrum. It can be stated that the frequency of

TABLE 6.1 Constructive Parameters Considered for the Calculus of Characteristic Frequencies of 6207 and 6209 Bearings

	Constructive parameters				Characteristic frequencies			
Tested bearing	D_m	D_b	z	a (°)	f_e (f_n)	f_I (f_n)	f_m (f_n)	f_c (f_n)
6207	54.5	9.922	8	0	3.272	4.728	2.655	0.409
6209	65	12.000	8	0	3.262	4.738	2.616	0.408

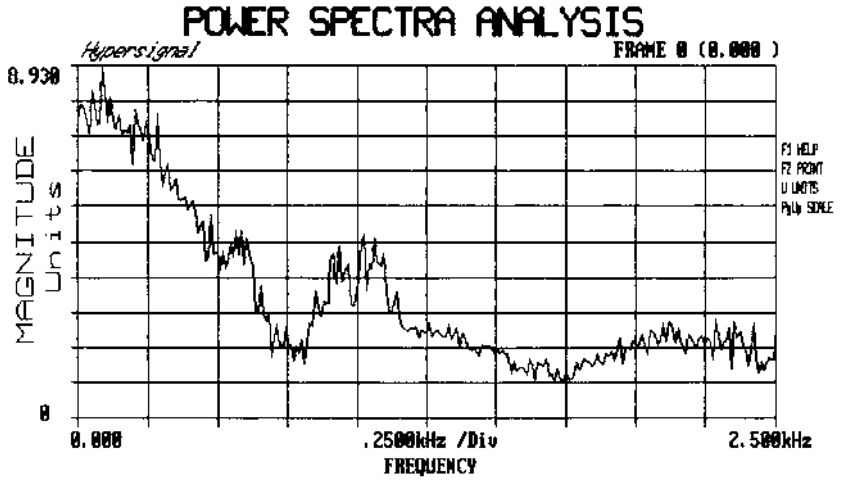

FIGURE 6.19 Power spectrum drawn on a 6207 bearing in a state of perfect functioning.

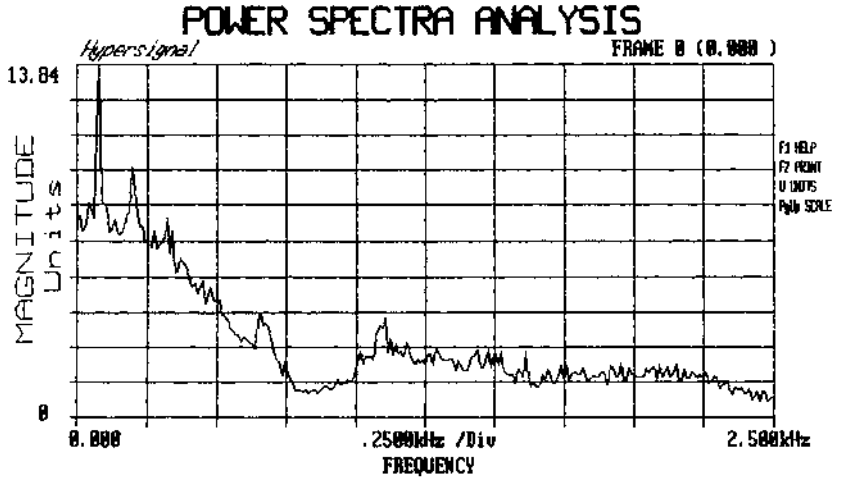

FIGURE 6.20 First signs of damage on the power spectrum drawn for the 6207 bearing.

balls rolling on the external tray and its superior harmonics that occur in the last captured power spectrum signalize the beginning of a fault on the external rolling path—a fact confirmed by the subsequent evolution of the fault.

The same identification method of mechanical defects was applied also in the case of the movement-transforming mechanism screw-nut with balls, for a damage simulated on the rolling path from the leading screw.

Table 6.2 presents the values of the constructive parameters that enter in the calculus of characteristic frequencies of the screw-nut with balls mechanism [relations (6.31) through (6.33)], and also the values of these frequencies, depending on the rotation frequency of the leading screw.

Figure 6.21 shows a power spectrum resulting from a vibration signal captured on the "clean" zone of the leading screw using an Emco acquisition system and Hypersignal software. Figure 6.22 presents a power spectrum of a new signal captured rolling the nut over the area with a simulated damage (pitting) on the leading screw. The maximum values from this last spectrum correspond to a frequency of 234.4 and 254 Hz, respectively.

For the measured rotational speed of the leading screw of 960 rot/min, the rotation frequency is $f_n = 16$ Hz, which leads to $f_s = 237.95$ Hz and $f_b = 253.63$ Hz, respectively, values of the characteristic frequencies. It is noticeable that even the power spectrum signals the occurrence of a damage by the significant increases in amplitude at characteristic frequencies; this time, it is not possible to locate the damage on one of the rolling paths. This behavior can be due to the play between the mechanism's elements.

In conclusion, the method of interpretation of the power spectrum is an efficient and rapid method of identification of mechanical defects—although their localization is, in some cases, more difficult. These reasons

TABLE 6.2 Values of the Constructive Parameters that Enter in the Calculus of Characteristic Frequencies of the Screw-Nut with Balls Mechanism

Constructive parameters				Characteristic frequencies (Hz)		
D_m	D_b	β	β'	f_s	f_p	f_b
30	3.00	35°	20°	14.872 f_n	15.825 f_n	3.355 f_n

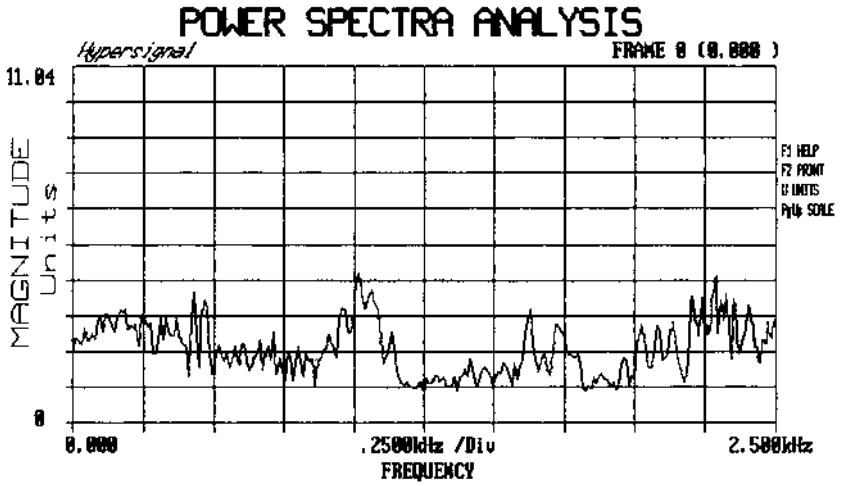

FIGURE 6.21 Power spectrum resulting from vibration signal captured on the "clean" zone of the leading screw using an Emco acquisition system and Hypersignal software.

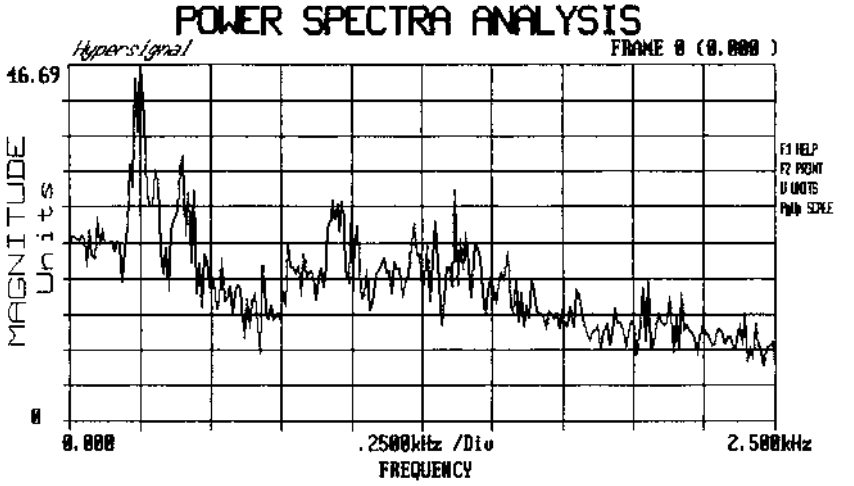

FIGURE 6.22 Power spectrum of a new signal captured rolling the nut over the area with simulated damage (pitting) on the leading screw.

led to the elaboration of the spectrum comparison method, which has shown excellent results in profoundness diagnosis. The theoretical presentation of this method can be found in Chapter 3 of this book.

6.6 EXPERIMENTAL RESEARCH IN VIRTUAL INSTRUMENTATION

6.6.1 Structure of Data Acquisition and Process System in Virtual Instrumentation

A data acquisition system has to be able to accomplish three fundamental functions: conversion of physical signal in a signal that can be measured; measurement of the signals generated by transducers/sensors to extract information; and construction of data analysis and data presentation in a useful form. A data acquisition and process system uses a computer (PC) as a process controller. Figure 6.23 presents the general structure of such a system, and this structure can be described as: transducers for conversion of the measured signal into a signal of electric nature; circuits to adapt the signal for isolation, conversion, and/or amplification of the signal coming from the transducer; a system of multiplexors and analogue–digital converters; and a calculus system with an adequate software.

The analogue–digital board (A/D) has the role of transforming the analogue signal (a continuous function in time), passed by the adapting circuit, in a numerical (discrete) format that can be processed by the

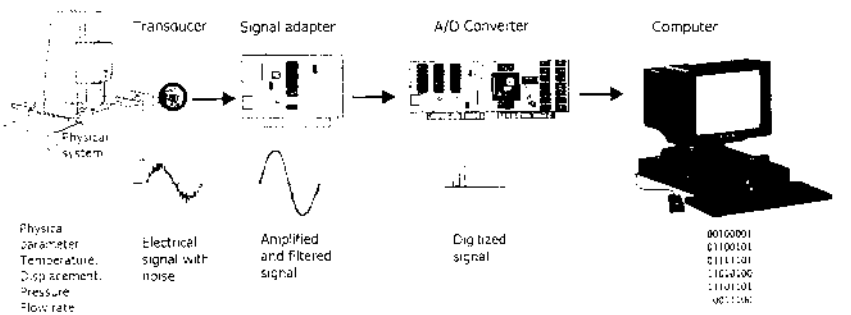

FIGURE 6.23 Data acquisition and process system using a computer (PC) as process controller.

computer. The analogue–digital conversion is a comparison operation; the signal is compared to a reference value, which is then represented as a codified digital number. There are a minimum and maximum number of samples that must be captured in order to optimize the accuracy of measurements. In the data acquisition and process system architecture, the role of the analogue–digital interface is very important because this interface must have a few essential functions for the user:

High speed data transfer to PC on the DMA (direct memory access) channel
Electronic part for starting the hardware and software
Amplification with programmable gain and noise filtration
Memory buffer

The operational system through which the virtual instrumentation presented in Chapter 5 was elaborated, tested, and then applied, contains: an IBM PC 486 computer (100 KHz, 16 Mb RAM), data acquisition board AT-MIO-16L-9 National Instruments, conditioning amplifier 2625 B&K, piezoelectric vibrations transducer 4344 B&K, LabVIEW 2.5 National Instruments software, and a real-time frequency analyzer 2034 B&K for testing virtual instruments. This system was provided by the S.C. Eurotest S.A. Laboratories, Seism-Vibrations department, together with their support and collaboration all throughout the experimental research.

6.6.2 Experimental Research in Surface Diagnostics

The virtual instruments for surface diagnosis FACVARF and INDDIAG, whose structure was presented in Chapter 5, have been used to monitor the evolution of mechanical damage on the radial ball bearing 6209. The experimental setup is similar to that presented in Figure 6.11, only the virtual instrumentation took the place of traditional equipment.

Figure 6.24, showing diagnosis in virtual instrumentation by the peak factor method, presents the front panel of the FACVARF virtual apparatus, which exhibits the reference acquisition graphic in the time domain, for the new bearing, and under this graphic, another graphic of a subsequent recording when the mechanical damage already started. In the graphic of peak factor evolution the spectacular decrease of the peak factor value from $F_v = 10.1$ to $F_v = 8.2$ is due to bearing lubrica-

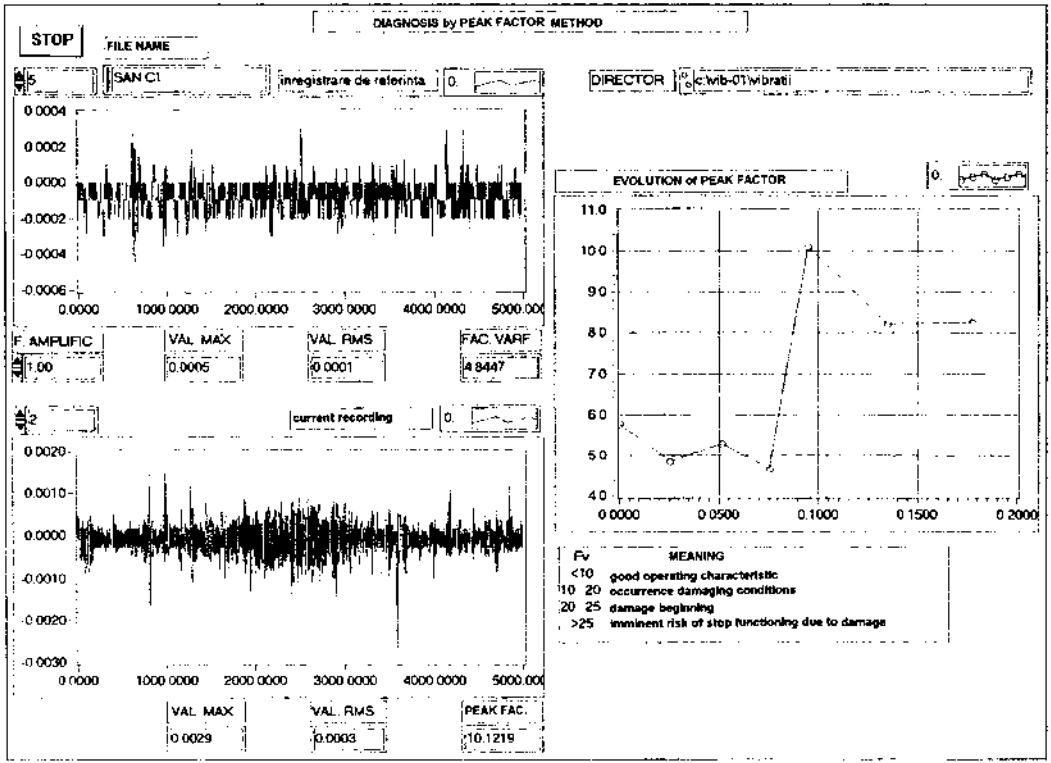

FIGURE 6.24 Diagnosis by peak factor method on the front panel of the FACVARF virtual apparatus.

tion, which had been mounted without lubricant to hasten the damage occurrence.

The INDDIAG virtual apparatus for the same monitoring and diagnosis operation was used simultaneously (Fig. 6.25). Data acquisitions were also made with the bearing in perfect functioning state after the damages started, and a diagnostic index evolution graphic was automatically drawn. Both front panels display a legend to facilitate the interpretation of results.

The Kurtosis method in virtual instrumentation (virtual apparatus INDKURT) was used in many diagnostic situations both in the case of ball bearings and the screw-nut with balls mechanism, because it is possible to estimate without knowing the machine's "history," the functioning state of the analyzed element. Figure 6.26 presents this method for diagnosis of the same bearing. The value of the Kurtosis index $\beta_2 = 3.59$ and the probability density distribution of the amplitude of the captured signal confirm that the bearing is in perfect functioning state.

Other front panels of the INDKURT virtual apparatus are presented in the appendices of this book for other diagnostic situations on the basis of the vibrator signal.

6.6.3 Experimental Research in Profoundness Diagnostics

The virtual apparatus MECOSPEC was presented in Chapter 5. This apparatus is destined to establish the technical diagnostic using the spectrum comparison method. Given the precision of this apparatus, noted during the laboratory tests, this virtual instrument was used during experimental research to monitor the functioning state of some needle bearings. The purpose of this action was to see if the calculus relations presented for determination of critical frequencies for the ball bearings were verified also in case of needle bearings.

Table 6.3 presents the constructive parameters that compete with the calculus of characteristic frequencies of bearings, and also the values of these frequencies, depending on the rotation frequency f_n of the inner ring. The characteristic frequencies were calculated using relations (6.12) to (6.14).

Figure 6.27 presents the captured signal in the time domain and passed in the frequency domain by a fast Fourier transform for a radial needle bearing NA 4909 in perfect functioning state. The resulting power spectrum is considered a reference spectrum and is used to obtain the warning template and alarm template, respectively.

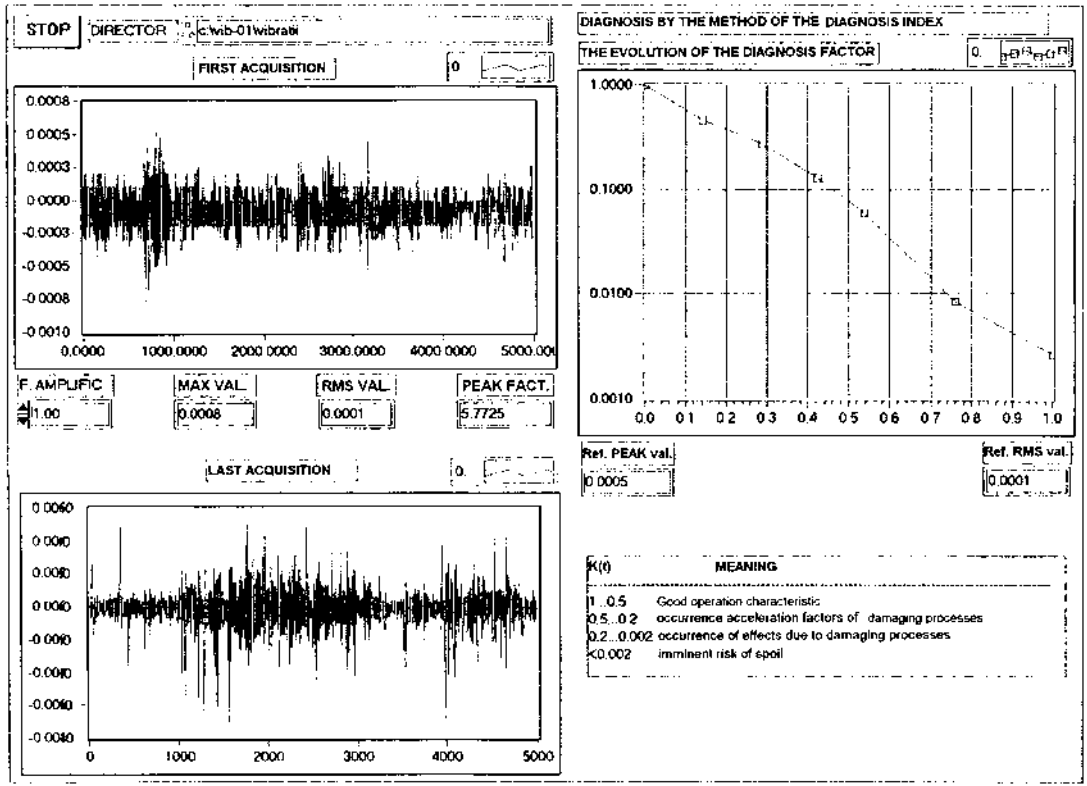

FIGURE 6.25 Diagnosis on the front panel of the INDDIAG virtual apparatus.

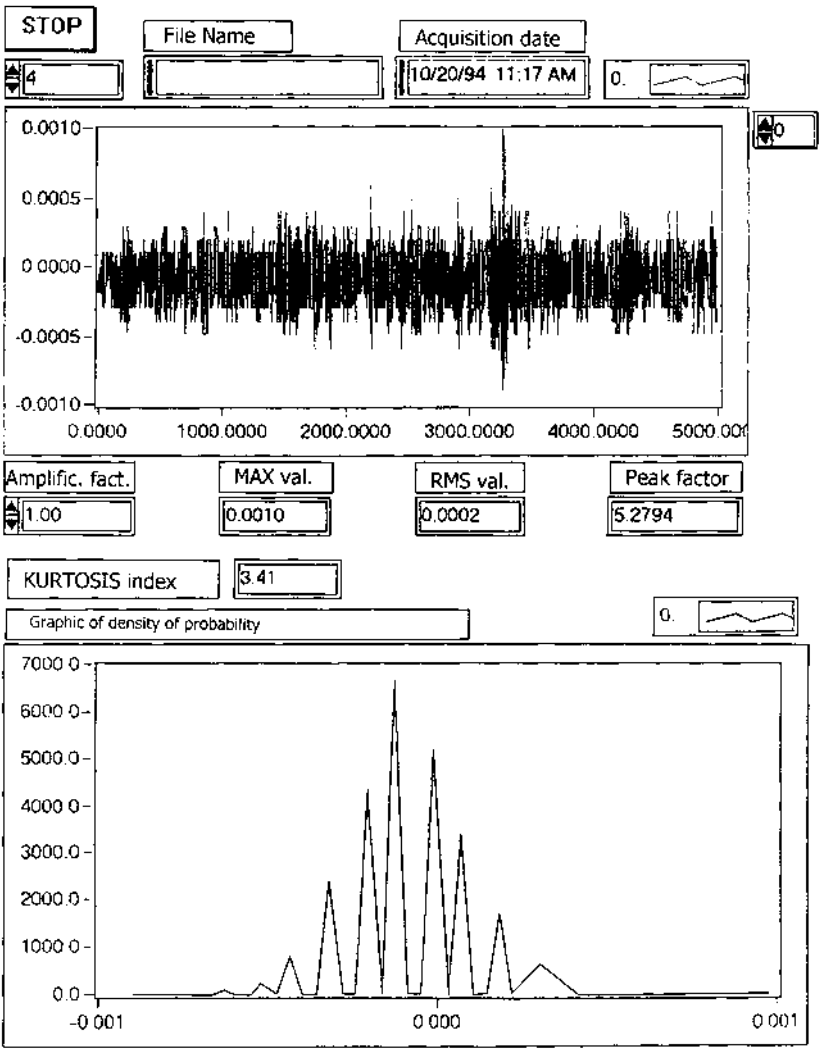

FIGURE 6.26 Kurtosis method in virtual instrumentation (virtual apparatus INDKURT).

TABLE 6.3 Constructive Parameters that Compete with the Calculus of Characteristic Frequencies of Bearings and the Frequency Values

	Constructive parameters				Characteristic frequencies		
Bearing type	D_m	d	z	β (°)	f_E (f_n)	f_I (f_n)	f_m (f_n)
NA 4907	45	3.5	27	0	12.45	14.55	6.39
NA 4908	51	3.5	29	0	13.00	15.50	7.25
NA 4909	56.5	4	25	0	11.62	13.38	7.03

The current spectrum is compared to these templates in the next section of the virtual diagnosis instrument. This way the warning template obtained by raising by the power two and side plating to the octave of the reference spectrum serves as a comparison element for a wear spectrum taken after the debut of mechanical damage (Fig. 6.28). The difference between the two spectra is graphically displayed to allow a direct read.

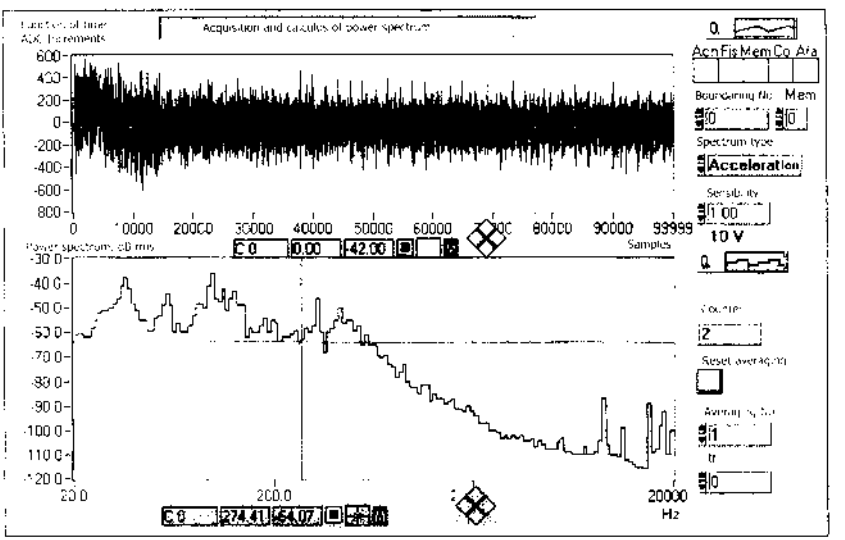

FIGURE 6.27 Captured signal in time domain and passed in frequency domain by FFT for radial needle bearing NA 4909 in perfect functioning state.

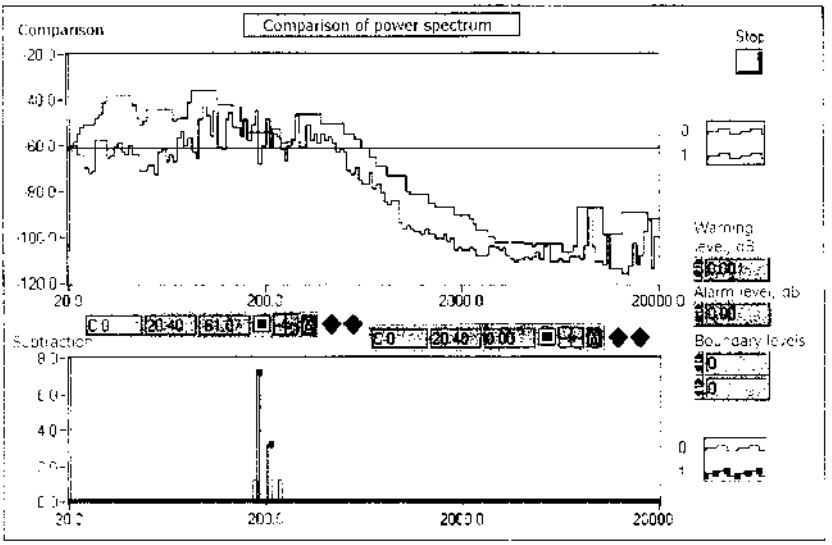

FIGURE 6.28 Warning template obtained by raising by the power two and side plating to octave of the reference spectrum serves as comparison element for wear spectrum taken after debut of mechanical damage.

During determinations only a few and the same frequencies have increased overpassing the alarm template, a phenomenon which is presented in Table 6.4. The characteristic frequencies calculated as a function of the input rotational speed $n = 960$ rpm ($f_n = 16$ Hz) applied to the inner ring are:

Rolling frequency of needles on the outer ring, $f_E = 185.92$ Hz
Rolling frequency of needles on the inner ring, $f_I = 214.80$ Hz
Rolling frequency of needles in the cage, $f_m = 112.48$ Hz

It can be stated that the relations for the calculus of the characteristic frequencies for one-row ball bearings can be applied also to radial needle bearings comparing the above calculated frequencies with those experimentally obtained (Table 6.4) by the intensive wear of the bearing on the test stand.

Figure 6.29 graphically presents the evolution of overpasses to the three frequencies mentioned in Table 6.4. It is considered that the evolution of the frequencies that signal the mechanical damage is approximately linear in the regime wear domain, so the points resulting from

Table 6.4 Comparing the Calculated Frequencies with Those Experimentally Obtained

Overpasses (dB) at read no.	7	9	11	13	15	17
Frequency (Hz)						
183	0.5	0.9	2.8	5.3	7.7	9.4
208	—	0.3	1.2	2.9	3.6	4.8
230	—	—	—	—	1.6	2.0

measurements can be interpolated to a line. At any moment, the time left until the stop by damage can be estimated by intersecting the interpolated line with the alarm level for the researched frequency.

In the last version of the virtual apparatus diagnosis MECOSPEC (Fig. 6.30) the spectrum comparison and supplementary processing of the warning template overpass is replaced with a representation type WATERFALL, which is a tridimensional representation made for the power spectra coming from successive captured signals at the same measuring point. At the spectrum axis, frequency and amplitude, the time axis is added. The spectra are successively represented on the time axis depending on the acquisition moment (Fig. 6.31). On this representation,

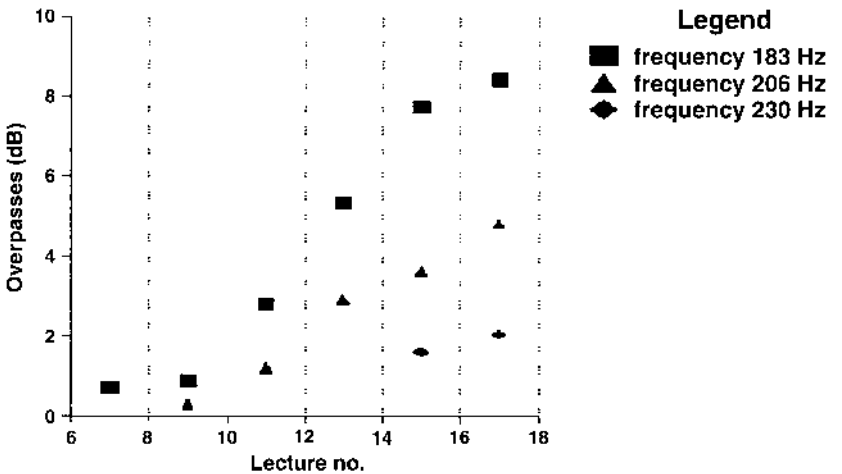

Figure 6.29 Evolution of overpasses to frequencies mentioned in Table 6.4.

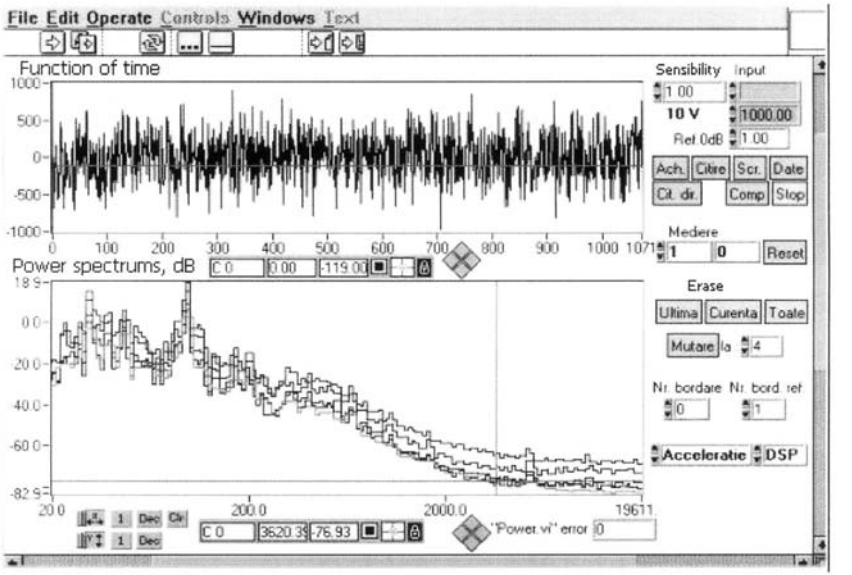

FIGURE 6.30 WATERFALL representation on the last virtual apparatus diagnosis MECOSPEC.

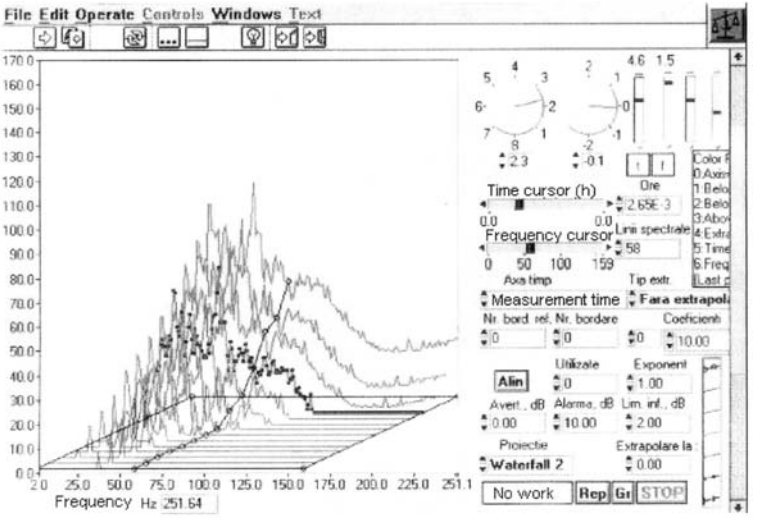

FIGURE 6.31 In the WATERFALL representation, the spectra are successively represented on the time axis depending on the acquisition moment.

with the aid of a time cursor any of the represented frequency spectra can be selected, and with the aid of a frequency cursor the evolution in time can be monitored for any frequency of the vibration signal from the power spectra.

6.6.4 Advantages of the Use of Virtual Instrumentation in Technical Diagnosis

The use of virtual instrumentation in monitoring and establishing of technical diagnosis offers special facilities to users as follows.

Visual Programming. This type of programming is primarily a rapid, sure, and easy path to the elaboration of special applications, adapted to imposed requests, easy to test and to maintain. It is the type of programming recommended to those who have not had the opportunity to familiarize themselves with a "classical" programming language. Instead of writing hundreds of rows of program, the user can build a program as a functional diagram choosing from the menu a series of visual elements that he or she logically interconnects. The rapidity and simplicity of the work stimulate conversion of traditional techniques of diagnosis and help find new virtual instrument techniques.

High Rate of Sampling. The rate of sampling (expressed in samples per second or sometimes in Hz) represents the measure of speed by which the A/D board can scan the input channel, and can identify the discrete value of the signal depending on the reference value. Theoretically, a data acquisition system must sample with a speed at least twice that of the largest frequency that can exist in the input signal; if this rule is not realized, a completely different wave shape will be obtained, having a smaller frequency, a phenomenon called aliasing. The high sample speeds that are reached at present rapidly load the computer memory but this phenomenon is no longer a problem due to the technological development of computers. The diagnostic problems need a medium level of sample rate that can be solved with 8 or 16 Mb RAM.

Good Resolution of Measurements. The resolution (expressed in percentages or bits) defines the smallest variation of the input signal that can be detected by the acquisition system. In virtual instrumentation a resolution comparable to that of dedicated traditional instruments produced by prestigious companies can be obtained.

Possibility of Choice of Sampling Mode. In applications of frequency analysis using FFT, any deviation in the period of time between sampling produces considerable errors. The acquisition system with virtual instrumentation realizes the start of the A/D converter (triggering) directly by the clock from the hardware or an external clock on the acquisition board. More than that, the possibility of choosing the pretrigger or posttrigger modes exists.

Data Transfer Speed. Using the direct memory access transfer mode the system takes over the data from the acquisition interface and puts these data directly in the computer's memory. DMA transfers are directly controlled by hardware and are extremely rapid. Ultrafast acquisition systems that use memory located directly on the acquisition plate also exist, so these systems will no longer be limited by the computer thoroughfare speed. In these conditions a "real-time" data process becomes possible, an accomplishment hard to achieve and expensive to realize with traditional instrumentation.

Possibility of Using the Multiplexor. The multiplexor is an electronic device that disposes more input channels, an output channel, and digital control inputs. Using these control inputs the needed input channel can be selected and connected to the output channel. The multiplexor is useful for supervising machines with a large number of measuring points, using the same measurement instrument.

Use of Work Programs with Annexed Apparatus (Driver-E Software). These work programs with annexed apparatus constitute a soft level that directly programs the acquisition hardware, administers the functioning of the acquisition hardware, and ensures integration with computer resources. They hide the complicated details of hardware programming, ensuring an easy to understand interface for the user.

Data acquisition systems tend to be more and more mass consumption goods because of the continuous technological improvement of this peak domain. These conditions determine the transformation software, an important factor related to data acquisition and process differentiation.